

# Numerical Assessment Of Temperature Distribution In Two Hot Air-Drying Chamber Geometries (Cuboid And Cylindrical)

MANGEH III FONDZENYUY Cedric<sup>1</sup>, Wu Mingliang<sup>1,2\*</sup>, Xiao Yao<sup>1</sup>, LOOH George ASHWEHMBOM<sup>1</sup>

<sup>1</sup>Department of agricultural mechanization engineering, college of engineering, Hunan Agricultural university, Changsha, Hunan province, 410128, P.R. China)

<sup>2</sup>Hunan Provincial Engineering Technology Research center for Modern Agricultural Equipment, Changsha, Hunan, 410128, P.R China)

Corresponding author's email: [mlwu@hunau.edu.cn](mailto:mlwu@hunau.edu.cn)

**Abstract** — During the drying process, enormous energy is required from both fuels and electrical sources to generate the heat energy required for drying. To economize the energy input during drying, it is important to design a dryer with an efficient temperature distribution inside the drying chamber. Computational Fluid Dynamics (CFD) was used to assess the temperature distribution through two different drying chamber geometries. This was done with aims of proposing an optimal geometry for a hot air dryer. Specifically, to determine the uniformity of temperature distribution in both geometries and then determine the heat loss to the seeds for the selected optimal geometry. In this research, numerical simulations were calculated using the RNG (re-normalization group) k-ε model equation for the cylindrical chamber geometry and the realizable model was used for the cuboid geometry. The two-drying chamber geometries were mathematically designed and meshed with curvature type advanced sizing function with mesh inflation controlled by the program. The simulations were then calculated from which temperature distribution within the two geometries were obtained and reported. The average exit temperatures for the geometries was about 330.25 K and 306.209 K for the cylindrical and cuboid geometries respectively. After selection, the heat lost to the seeds was determined to be 279.698 KJ for the cylindrical geometry. Using this software, the geometry of the hot air dryer chamber was selected. The geometry had a more uniform temperature distribution which in turn improves efficiency of the dryer, reduces drying time and further reduce energy consumption during drying.

**Keywords**—numerical; assessment; drying chamber; temperature distribution; Computational fluid dynamics; thermal equilibrium; rapeseed drying; cyclone dryer;

## I. INTRODUCTION

Large demands of the drying industry constantly push the development of new technologies and equipment [1]. Drying is an essential post-harvest process which helps to reduce loss by reducing water activity of

produce to a level below which deterioration doesn't occur for a definite period of time [2]. The rate of drying is determined by grain moisture content (MC) and temperature as well as temperature, relative humidity and velocity of the air in contact with the grains. Temperature and humidity are directly proportional ( $T \propto h$ ) and influence moisture removal capacity of the drying air. During drying, enormous energy is required from both fuels and electrical sources to generate the heat energy required. To economize energy input during drying, it is important to design a dryer with an efficient temperature distribution inside the drying chamber [3]. In the course of this research, CFD (Computational Fluid Dynamics) was used to assess the temperature distribution through two different drying chamber geometries in order to select a geometry with a more uniformly distributed temperature to be used in the dryer. CFD is a cost and time effective way of studying the air flow fields and temperature distributions within fluid flow systems and it provides parameters that are not easy to come by experimentally. CFD has been used by lots of researchers in the recent years to study temperature distribution and air flow fields in fluid flow systems. Jose L et al [3] used CFD analysis to improve the temperature distribution in a chili dryer considering the effects of continuous air speed to guarantee uniformity within the drying chamber with minimum energy consumption. Cristiana B et al [2] did a simulation of the airflow inside a hybrid dryer using CFD commercial package and their numerical results were in agreement with experimental results inside the uncertainty range of temperature sensors. Qixia Y et al [4] did simulations and analysis on the temperature distribution of the heating channel in a washer-dryer using ANSYS Fluent and noticed that, the uneven velocity distribution surrounding the heater leads to the transverse offset and the triangular hump and downstream bend lead to the longitudinal offset which provide proper theoretical foundations for further production and modifications. Hana C et al [5] used computer simulations to study the temperature distribution during the cooling process of a thermally insulated room. Also, AG Niam et al [6] used CFD simulations to compute temperature distribution and pattern with two alternate positions of the air conditioners. They used the numerical method to verify the results of the calculation which used the

grid convergence index. Y. Amanlou et al [7] used CFD to envisage geometries of a cabinet dryer in an attempt to obtain a uniform distribution of drying airflow and temperature. In 2012, Lars B et al [8] used CFD to optimize a pellet burner by studying the temperature and air distribution along the combustion chamber in order to improve the burning efficiency omitting the chemical reactions involved during burning. In 2015, Zdanski et al [9] numerically assessed the air flow behavior in a convectional compact dry kiln in which they aimed to recommend a design with the highest possible level of flow uniformity across the lumber stack of the kiln. In 2010, Low A. et al [10] using CFD during their investigation of heat and mass transfer in a solar dryer deduced that heat and mass transfer by natural convection is more suitable for drying pepper berries with solar radiation. Miguel A et al [1] conveyed a numerical analysis of a convective drying chamber from drying air velocity and temperature perspective and their established procedure was set up with the aim of evaluating the distribution of drying air velocity and temperature on the drying chamber to define the need of redesigning it. Marian V et al [11] in 2014 predicted the air flow and temperature profiles inside a convective solar dryer. They did a numerical simulation with CFD using a reduced 2-Dimensional (2D) domain model neglecting effects from side walls.

The main aim of this research was to propose an optimal geometry for a hot air dryer. Specifically, we had to determine the uniformity of temperature distribution in both cuboid (layer) and cylindrical (cyclone) geometries and further determine the heat loss from the hot air to the seeds (heat transfer) for the selected optimal geometry. It is important to note that during this study, it is assumed that the heat lost to the atmosphere through the drying chamber walls is negligible. In line with attaining these objectives, the following materials and methods were employed.

## II. MATERIALS AND METHODS

### A. The governing equations

Heat and mass transfer during the drying process were accomplished by solving both the continuity, momentum and energy equations using the dryer boundary conditions. The expressions for mass, momentum and energy conservation are stated below [2]:

$$\frac{\partial \rho}{\partial t} + \vec{\nabla} \cdot (\rho U) = 0 \quad (1)$$

$$\frac{\partial(\rho U)}{\partial t} + \vec{\nabla} \cdot (\rho U \otimes U) = -\vec{\nabla} p' + \vec{\nabla} \cdot (\mu_{eff}(\vec{\nabla} U)) + B \quad (2)$$

$$\frac{\partial(\rho h_{tot})}{\partial t} - \frac{\partial p}{\partial t} + \vec{\nabla} \cdot (\rho U h_{tot}) = +\vec{\nabla} \cdot (k(\vec{\nabla} T)) + S_E \quad (3)$$

In which cases,  $\mu_{eff}$  is the turbulent effective viscosity,  $S_E$  the energy source term,  $p'$  the modified pressure and  $B$  is the sum of body forces.  $\mu_{eff}$  and  $p'$  are given

by:

$$\mu_{eff} = \mu + \mu_t \quad (4)$$

And

$$p' = p + \frac{2}{3} \rho k \quad (5)$$

Total specific enthalpy ( $h_{tot}$ ), pressure ( $p$ ) and thermal conductivity ( $k$ ) are related by the expression

$$h_{tot} = h + \frac{1}{2} U^2 \quad (6)$$

In this research, the numerical simulations were calculated using the RNG (re-normalization group)  $k$ - $\epsilon$  model equation for the cylindrical chamber geometry and the realizable model was used for the cuboid geometry. This was advantageous because the effect of swirl on turbulence is included in the RNG model, enhancing accuracy for swirling flows and provides an analytically-derived differential formula for effective viscosity that accounts for low-Reynolds number effects. The realizable model on the other hand modified the transport equation for the dissipation rate,  $\epsilon$ , which has been derived from an exact equation for the transport of the mean-square vorticity. With this modification, the model satisfies certain mathematical constraints on the Reynolds stresses which is consistent with the physics of turbulent flows.

### B. Transport Equations for the RNG $k$ - $\epsilon$ model and Realizable $k$ - $\epsilon$ model

The RNG  $k$ - $\epsilon$  model has a similar form to the standard  $k$ - $\epsilon$  model expressed as:

$$\frac{\partial(\rho k)}{\partial t} + \frac{\partial(\rho k u_i)}{\partial x_i} = \frac{\partial(\alpha_k \mu_{eff} \frac{\partial k}{\partial x_j})}{\partial x_j} + G_k + G_b - \rho \epsilon - Y_M + S_k \quad (7)$$

And

$$\frac{\partial(\rho \epsilon)}{\partial t} + \frac{\partial(\rho \epsilon u_i)}{\partial x_i} = \frac{\partial(\alpha_\epsilon \mu_{eff} \frac{\partial \epsilon}{\partial x_j})}{\partial x_j} + C_{1\epsilon} \frac{\epsilon}{k} (G_k + C_{3\epsilon} G_b) - C_{2\epsilon} \rho \frac{\epsilon^2}{k} - R_\epsilon + S_\epsilon \quad (8)$$

Meanwhile the modeled transport equations for  $k$  and  $\epsilon$  in the realizable  $k$ - $\epsilon$  model are:

$$\frac{\partial(\rho k)}{\partial t} + \frac{\partial(\rho k u_j)}{\partial x_j} = \frac{\partial((\mu + \frac{\mu_t}{\sigma_k}) \frac{\partial k}{\partial x_j})}{\partial x_j} + G_k + G_b - \rho \epsilon - Y_M + S_k \quad (9)$$

And

$$\frac{\partial(\rho \epsilon)}{\partial t} + \frac{\partial(\rho \epsilon u_j)}{\partial x_j} = \frac{\partial((\mu + \frac{\mu_t}{\sigma_\epsilon}) \frac{\partial \epsilon}{\partial x_j})}{\partial x_j} + \rho C_{1\epsilon} S_\epsilon - \rho C_{2\epsilon} \frac{\epsilon^2}{k + \sqrt{v \epsilon}} + C_{1\epsilon} \frac{\epsilon}{k} C_{3\epsilon} G_b + S_\epsilon \quad (10)$$

Where

$$C_1 = \max \left[ 0.43, \frac{\eta}{\eta + 5} \right], \eta = S \frac{k}{\epsilon}, S = \sqrt{2 S_{ij} S_{ij}} \quad (11)$$

In these equations,  $G_k$  represents the generation of turbulence kinetic energy due to the mean velocity gradients, calculated by:

$$G_k = -\rho \overline{u'_i u'_j} \frac{\partial u_j}{\partial x_i} \quad (12)$$

$G_b$  Is the generation of turbulence kinetic energy due to buoyancy given by;

$$G_b = \beta g_i \frac{\mu_t}{Pr_t} \frac{\partial T}{\partial x_i} \quad (13)$$

Where  $Pr_t$  is the turbulent Prandtl number for energy and  $g_i$  is the component of the gravitational vector in the  $i^{th}$  direction. The coefficient of thermal expansion,  $\beta$  is defined as:

$$\beta = -\frac{1}{\rho} \left( \frac{\partial \rho}{\partial T} \right)_p \quad (14)$$

Since we are dealing with an ideal gas (air), the generation of turbulence due to buoyancy reduces to:

$$G_b = -g_i \frac{\mu_t}{\rho Pr_t} \frac{\partial \rho}{\partial x_i} \quad (15)$$

In ANSYS Fluent,  $C_{3\varepsilon}$  is not specified but is instead calculated using the expression;  $C_{3\varepsilon} = \tanh \left| \frac{v}{u} \right|$  where  $v$  is the component of the flow velocity parallel to the gravitational vector and  $u$  is the component of the flow velocity perpendicular to the gravitational vector. This implies that  $C_{3\varepsilon}$  becomes 1 for buoyant shear layers for which the main flow is aligned with the direction of gravity.

$Y_M$  Represents the contribution of the fluctuating dilatation in compressible turbulence to the overall dissipation rate defined as:

$$Y_M = 2\rho\varepsilon M_t^2$$

Where  $M_t$  is the turbulent Mach number, defined as

$$M_t = \sqrt{\frac{k}{a^2}} \text{ And } a (\equiv \sqrt{\gamma RT}) \text{ is the speed of sound.}$$

The quantities  $\alpha_k$  and  $\alpha_\varepsilon$  are the inverse effective Prandtl numbers for  $k$  and  $\varepsilon$  respectively.  $S_k$  And  $S_\varepsilon$  are user-defined source terms. The scale elimination procedure in the RNG theory results in a differential equation for the modeled effective turbulent viscosity:

$$d \left( \frac{\rho^2 k}{\sqrt{\varepsilon \mu}} \right) = 1.72 \frac{\hat{v}}{\sqrt{\hat{v}^3 - 1 + C_v}} d\hat{v} \quad (16)$$

Where

$$\hat{v} = \frac{\mu_{eff}}{\mu}$$

$$C_v \approx 100$$

Turbulence, in general, is affected by rotation or swirl in the mean flow. The RNG model in ANSYS Fluent provides an option to account for the effects of swirl or rotation by modifying the turbulent viscosity appropriately. The modification takes the following functional form for RNG and realizable  $k-\varepsilon$  models respectively:

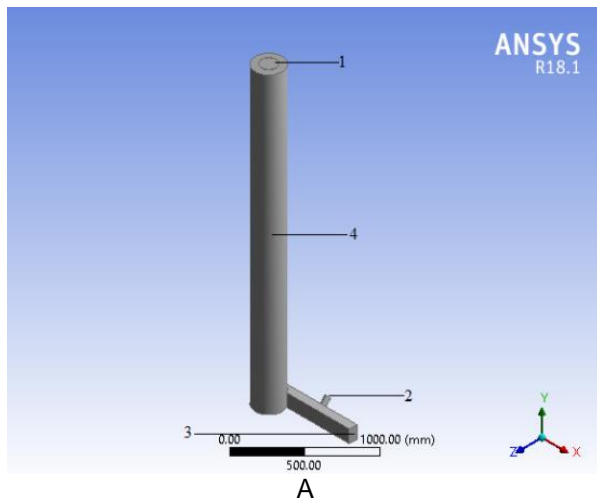
$$\mu_t = \mu_{t0} f \left( \alpha_s, \Omega, \frac{k}{\varepsilon} \right) \text{ and } \mu_t = \rho C_\mu \frac{k^2}{\varepsilon}$$

Where  $\mu_t$  is the value of turbulent viscosity,  $\Omega$  is a characteristic swirl number evaluated within ANSYS Fluent, and  $\alpha_s$  is a swirl constant that assumes different values depending on whether the flow is swirl-dominated or only mildly swirling. This swirl modification always takes effect for axisymmetric, swirling flows and three-dimensional flows when the RNG model is selected. For mildly swirling flows (the default in ANSYS Fluent),  $\alpha_s$  is set to 0.07. For strongly swirling flows, however, a higher value of  $\alpha_s$  can be used.

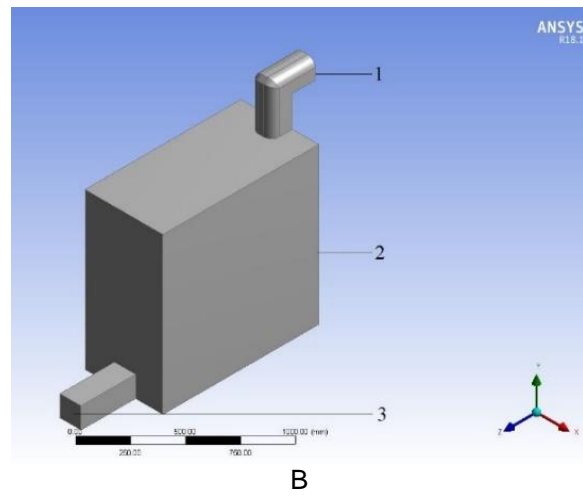
The model constants used in the calculations included  $C_{1\varepsilon} = 1.42$  and  $C_{2\varepsilon} = 1.68$  derived analytically by the RNG theory while  $C_{1\varepsilon} = 1.44$ ,  $C_2 = 1.9$ ,  $\sigma_k = 1.0$  and  $\sigma_\varepsilon = 1.2$  are used for the realizable  $k-\varepsilon$  model

### C. Design of the drying chamber and meshing

The two-drying chamber geometries were mathematically designed in the design modeler component system of ANSYS workbench. The designed geometries are presented on Fig. 1 below. After the design was complete, it was loaded into the meshing tool of ANSYS where the discrete cells were created.



A: 1. Pressure outlet 2. Rapeseed feed port 3. Velocity inlet of Ram 4. Drying cylinder



B: 1. Pressure outlet 2. Body within which the drying racks are placed 3. Velocity inlet for hot air

Figure 1: geometry of the drying chamber geometries

For meshing, the curvature type advanced sizing function with a fine relevance center and curvature normal angel of  $10^\circ$  were used. The inflation of the meshing was left to be controlled by the program. Max face and max tetrahedral sizes of  $2.4 \times 10^{-2}$  m and  $2.5 \times 10^{-2}$  m were both employed for both cylindrical and cuboid geometries (Fig. 2).

002 m were both employed for both cylindrical and cuboid geometries (Fig. 2).

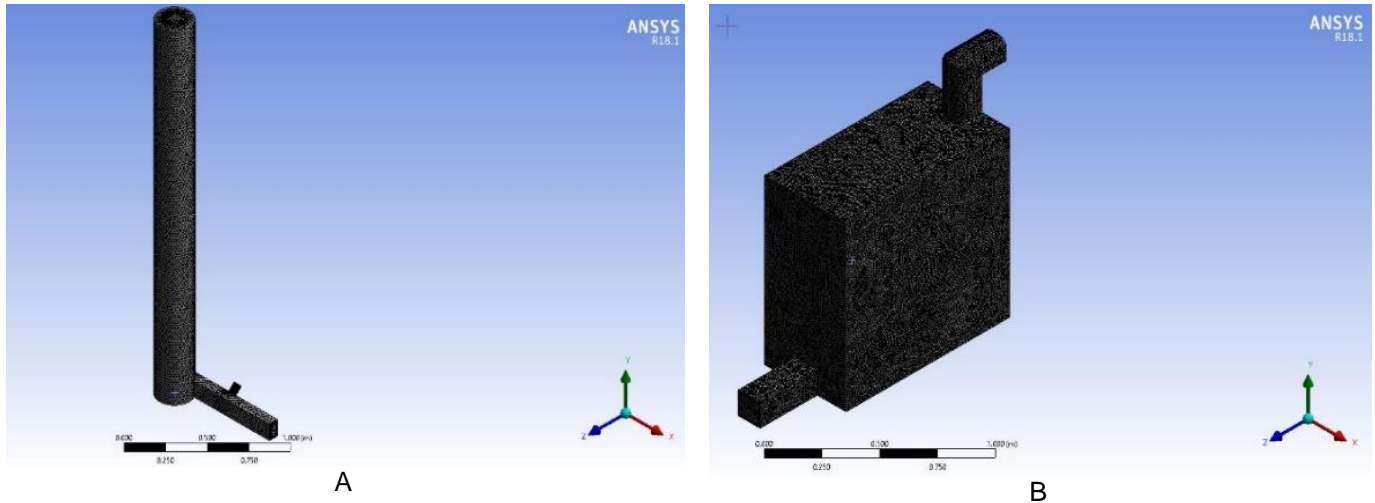


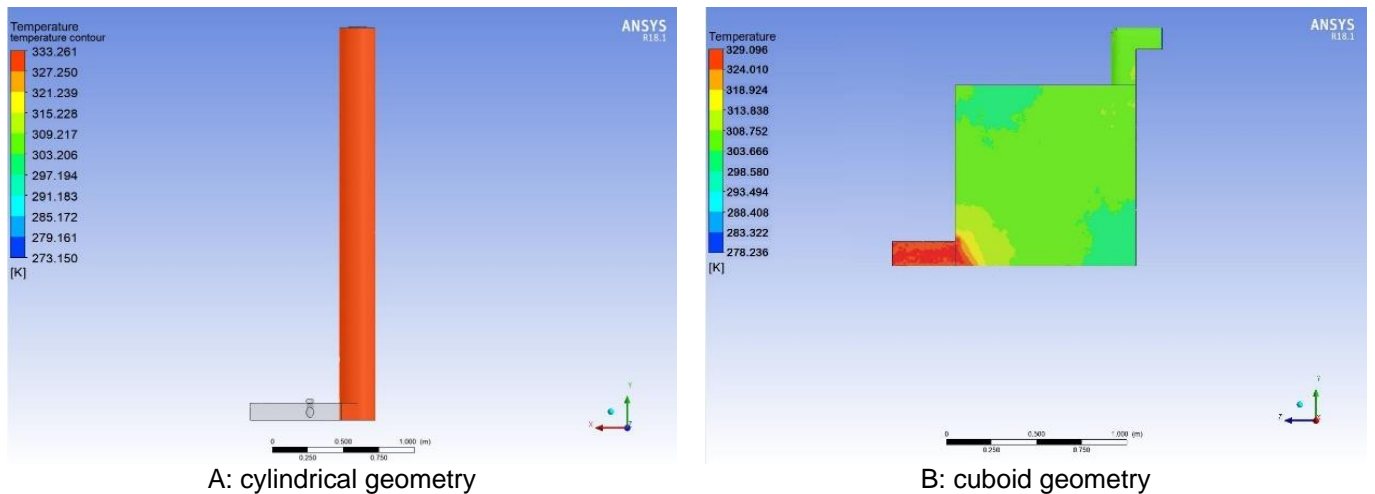
Figure 2: meshed drying cylinder ready for calculation of solutions

The simulations were run using an intel® core™ i5-8250U CPU @1.60GHz (8CPUs) computer, with 8 GB memory, requiring a Central Processing Unit (CPU) time range of about 1 hour 30 minutes to 2 hours. With the parameters set, the solution was initialized and run with 250 iterations. The density of the seeds was  $690 \text{ kg m}^{-3}$  and the specific heat capacity  $C_p = 1652.8 \text{ J kg}^{-1} \text{ K}^{-1}$ . The heat flux of the body-wall boundary was set to  $0 \text{ w m}^{-2}$ . The flow was scaled by the surface with a mass flow rate of  $1 \times 10^{-20} \text{ kg s}^{-1}$ . The convergence criteria

were set to  $1 \times 10^{-5}$  for the continuity equation,  $1 \times 10^{-6}$  for the energy equation and  $1 \times 10^{-3}$  for k-e equations respectively. The solution was then initialized at the inlet velocity surface for the hot air and calculations done.

### III. RESULTS

From the numerical calculations done, the temperature distribution within the two geometries were obtained and are presented in fig. 3.



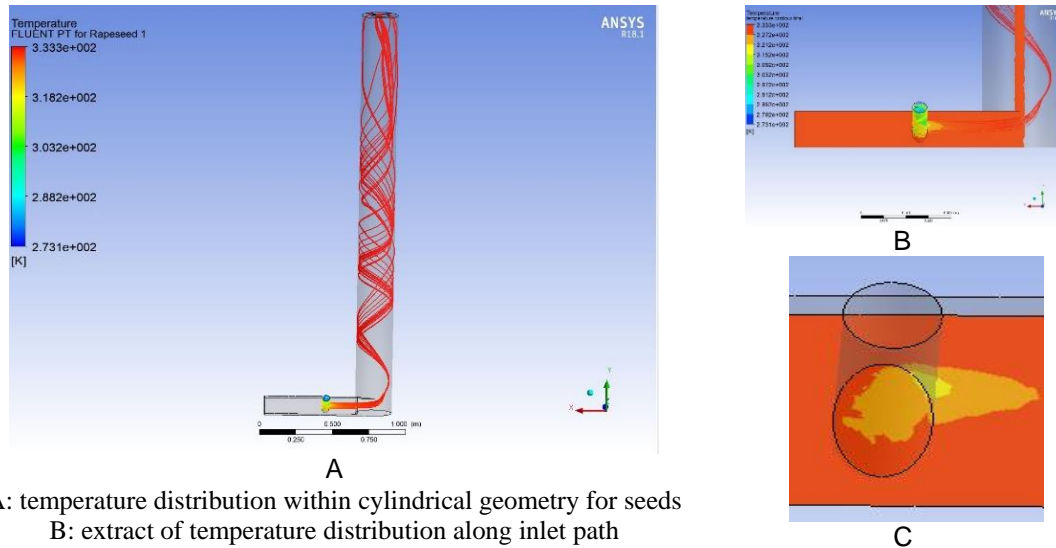
A: cylindrical geometry

B: cuboid geometry

Figure 3: temperatures distributions within the drying chamber geometries

The average exit temperatures in geometries were 330.25 K and 306.209 K for the cylindrical and cuboid geometries respectively. This average exit temperature and temperature distribution pictures above show that temperature is more uniformly distributed in the

cylindrical drying chamber geometry. For the cylindrical system which has a more uniformly distributed temperature, when the seeds were injected into the dryer, temperature distribution observed for the seeds was as presented on figure 4.



A: temperature distribution within cylindrical geometry for seeds  
 B: extract of temperature distribution along inlet path  
 C: rapid heat transfer upon contact of the seeds and hot air

Figure 4: temperature distribution on seeds within the cylindrical geometry

The temperature variation of the seeds during the drying is presented on Fig. 5 below.

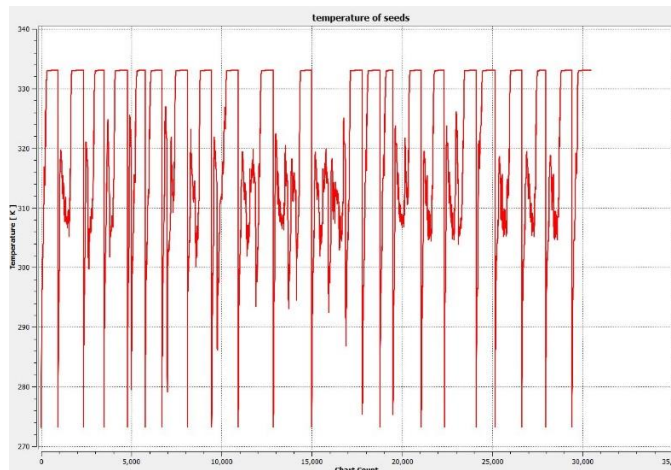


Figure 5: temperature variation of seeds during drying in the cylindrical geometry

The heat lost to the seeds is defined by:

$$Q = MC_p\Delta T$$

Where

$Q$  is the heat loss,

$M$  is Mass of seeds drying,

$C_p$  the specific heat

$\Delta T$  seed temperature difference

The temperature difference of the seeds is the difference between the initial temperature of the seeds (273.15 K) and the temperature of the seeds at equilibrium (330.25 K), and  $C_p = 1632.8 \text{ J Kg}^{-1} \text{ K}^{-1}$ . For a 3 Kg mass of seed sent in at a time, the heat gained by the seeds which is equal to the heat lost by the hot air will be:

$$Q = 3kg * 1632.8 \frac{J}{kgK} * (330.25 K - 273.15 K)$$

$$Q = 279.698 \text{ KJ}$$

Velocity within the cylindrical geometry from Fig. 6 and 7 below ranged from about  $0.1 \text{ ms}^{-1}$  to  $19.39 \text{ ms}^{-1}$ . Presented below is the velocity streamline, distribution of seeds, and contours.

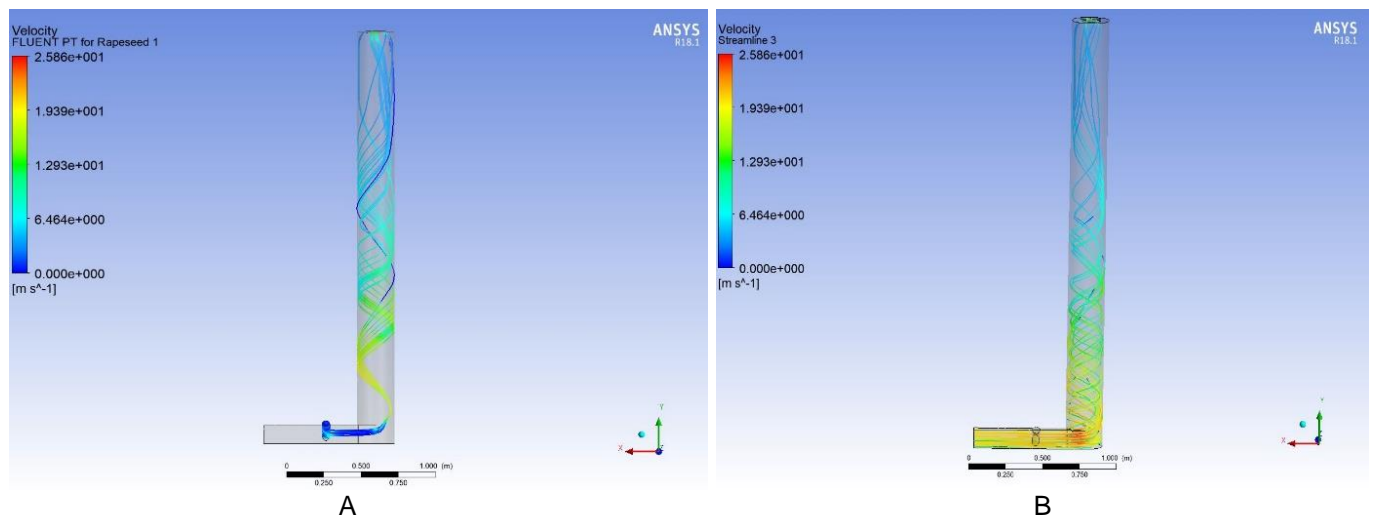


Figure 6: Velocity distribution of the seeds (A) and velocity streamline (B)

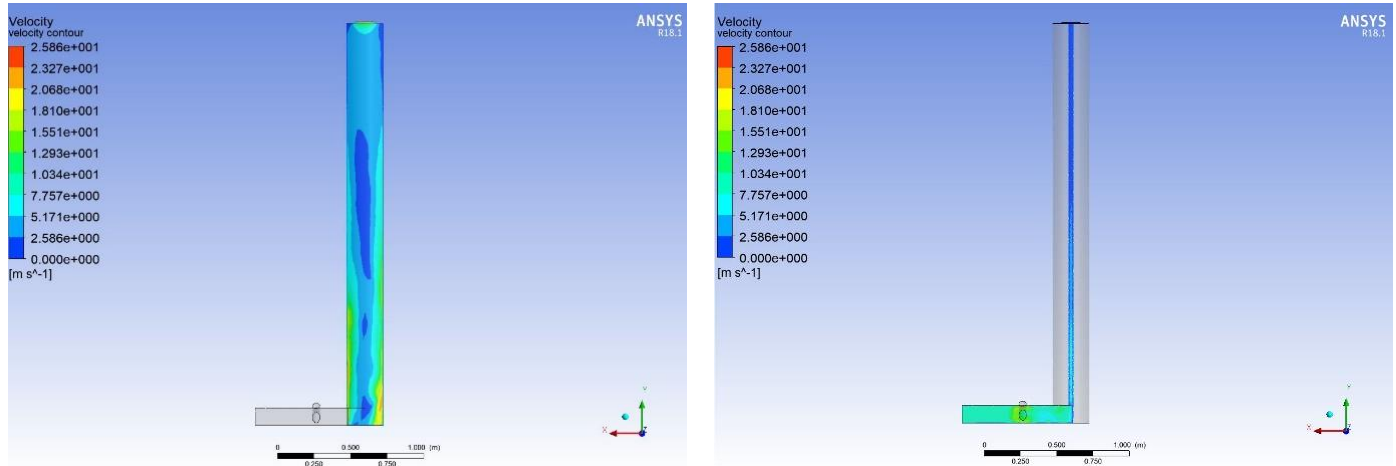


Figure 7: Velocity contours within the cylinder (A) and velocity contour at the vent (B)

#### IV. DISCUSSIONS

It is important to note that, due to different drying methods, inlet air speeds were different for the two geometries. Initial temperatures were 333.15 K (60°C) for both and the inlet speed for the cylindrical geometry was 20 m s<sup>-1</sup> (most of the kinetic energy is needed to move the seeds up the cylinder) while the air inlet speed for the cuboid geometry was 10 m s<sup>-1</sup> (lower than that for the cylinder to avoid the air from blowing away the seeds off the trays). Fig. 3 shows the temperature distribution at a cross section and symmetry in both geometries. The average exit temperatures for both geometries were 330.25 K and 306.209 K for the cylindrical and cuboid geometries respectively. This average exit temperature and temperature distribution pictures above show that temperature is more uniformly distributed in the cylindrical drying chamber geometry relative to the cuboid geometry. This uniformity in the cylindrical geometry is because of the size and shape differences (cylindrical geometry is more compact than the cuboid geometry). The cylindrical geometry attains thermal equilibrium faster for the same heat energy supplied considering that heat loss to the environment is negligible in both cases. Also, the modes of drying in the two geometries differ and influence temperature and velocity distribution. The cylindrical geometry uses a cyclone-like drying method. During drying, the seeds in the cylinder keep gyrating until they attain a safe moisture content before escaping through the classifier of the chamber. During this process, heat is transferred from the hot air to the seeds directly and just a short time is needed for the heat transfer process ( $C_p$  (specific heat capacity of seeds) = 1632.8 J Kg<sup>-1</sup> K<sup>-1</sup>). For the cuboid geometry, seeds are dried in trays placed in stacks with hot air passing through the trays. Inlet hot air passes through the seed masses in the trays and sweeps away the moisture. From calculations, average exit temperatures showed that more heat was lost within the cuboid geometry possibly because both seeds, stacks and trays gained some heat energy during drying. With this distribution and method of drying, seeds dried in the cylindrical system will have a more uniform final moisture content, a faster drying rate and more energy will be saved as compared

to the cuboid shaped drying chamber. For a more uniform distribution in the cuboid geometry to be attained, it is required that the pressure outlet be constricted and a diffusion of about 45° – 60° should be introduced at the velocity inlet. Temperature distribution within the cylindrical geometry will be influenced by a larger diameter, longer height and a smaller velocity inlet area. Considering these odds, a cylindrical geometry is more suitable for use in the designed dryer. Displayed in Fig. 4 above is the temperature distribution on the seeds during the drying process in the cylindrical drying chamber geometry. From fig. 4 we can observe that heat energy is gained by the rapeseed very rapidly which is accounted for by the low  $C_p$  (the heat required to raise the temperature of the unit mass) of rapeseed ( $C_p = 1632.8 \text{ J Kg}^{-1} \text{ K}^{-1}$ ). With this, it is very easy for the rapeseed to attain a thermal equilibrium with the hot air coupled with the advantage of the cylindrical cyclone drying method and compact geometry. Looking at the rapeseed inlet, the temperature of the seeds is still very low (about 273.15 K ± 1.5 K) and is mostly colored blue. Once the seeds get in contact with the incoming air, heat transfer occurs and the temperature of the seeds rise. Figure 4C shows the phase along the intake ram where the heat transfer occurs with the yellowish-orange color. The temperature of the seeds during the entire drying process ranges between 273 K to 330.5 K as presented on fig. 5. Lastly from the velocity distribution streamline and contours on fig. 6 and fig. 7 respectively, the seed velocity dropped continuously due to effect of gravity.

#### V. CONCLUSIONS

Designing dryers with a uniform temperature distribution is a great way of reducing the energy consumption during drying, improve final moisture content (MC) uniformity and also improve the drying rate. This study, was aimed at choosing from two drying chamber geometries by specifically calculating the temperature distribution within the chambers and further calculating the heat loss to the seeds in the selected system. From the results of numerical calculations, the cylindrical geometry was selected over the cuboid geometry based on the uniform distribution of steady state temperatures within the geometries, the uniformity

of final MC and faster drying rates. One of the desirable features of the cylindrical geometry was that the velocity and the temperature of the airflow were nearly uniform and homogenous in the drying chamber which is suitable for dryer purposes, since it guarantees a high-quality and homogeneous drying process [2]. The heat loss by the air to the seeds (heat energy gained) was also calculated at 279.698 KJ. The assessment of the airflow inside these geometries were done using CFD software ANSYS V18.1. Using this software, the geometry of the hot air dryer chamber was selected. The geometry had a more uniform temperature distribution which in turn improves efficiency of the dryer, reduces drying time and further reduce energy consumption during drying.

## References

- [1] Miguel Andres Daza Gomez, Carlos Andres Gomez Velasco, Nicolas Ratkovich, Juan Carlos Gomez Daza, "Numerical Analysis of a Convective Drying Chamber from Drying Air Velocity and Temperature Perspective," in *proceedings of the 3rd world congress on Momentum, heat and Mass transfer*, Budapest, Hungary, 2018.
- [2] Cristiana Brasil Maia, Andre Guimaraes Ferreira, Luben Cabezas-Gomez, Sergio de Moraes Hanroit & Tiago de Oliveira Martins, "Simulation of the airflow inside a hybrid dryer," *Internationl journal of Recent Research and Applied Studies*, vol. 3, no. 10, 2012.
- [3] Jose L. CARRERA ESCOBEDO, Arquimedes ORTIZ RIVERA, Cesar H. GUZMAN VALDIVIA, Mario A. GARCIA RUIZ and Omar DESIGA ORENDAY, "CFD ANALYSIS FOR IMPROVING TEMPERATURE DISTRIBUTION IN A CHILI DRYER," *Journal of thermal science*, vol. 22, pp. 255-267, 2016.
- [4] Qixia You, Fei lu, Yunfei Chen, and Jianrun Zhang, "simulation and analysis on the temperature distribution of the heating channel in a washer-dryer," *Journal of Applied Mechanics and Materials*, vol. 437, pp. 226-230, 2013.
- [5] Hana Charvatova, Ales Prochazka, and Martin Zalesak, "computer simulation of temperature distribution during cooling og a thermally insulated room," 19 November 2018.
- [6] AG Niam, TR Muharam, S Widodo, M Solahudin, L Sucahyo, "CFD Simulation Approach in Determining Air Conditioners position in the Mini Plant Factory for Shallot Seed Production," in *the 10th International Meeting of Advances in Thermofluids*, 2018.
- [7] Y. Amanlou, A. Zomorodian, "Applying CFD for designing a new fruit cabinet dryer," *Journal of Food Engineering*, vol. 101, pp. 8-15, 2010.
- [8] Lars B. WESTERLUND, Roger L. HERMANSSON, and Michel J. CERVANTES, "Computational Fluid Dynamics Optimisation of a Pellet Burner," *Thermal science*, vol. 16, no. 4, pp. 1175-1186, 2012.
- [9] P. S. B Zdanski, D. G. Possamai, and M. Vaz. Jr, "A Numerical Assessment of the Airflow Behaviour in a Conventional Compact Dry Kiln," *Journal of Applied Fluid Mechanics*, vol. 8, no. 3, pp. 367-376, 2015.
- [10] Low, Andrew R. H. Rigit and Patrick T. K., "Heat and Mass Transfer in a Solar Dryer with Biomass Backup Burner," *international Journal of Mechanical, Aerospace, Industrial, Mechatronic and Manufacturing Engineering*, vol. 4, no. 2, 2010.
- [11] Marian VINTILA, Adrian-Gabriel GHAIUS, Viorel FATU, "Prediction of Air Flow and Temperature Profiles inside Convective Solar Dryer," *Bulletin USDVM Food Science and Technology*, vol. 71, no. 2, 2014.

## Acknowledgment

I would like to express my special appreciation and thanks to my tutor Professor Wu Mingliang, you have been a tremendous mentor for me. I would like to thank you for encouraging my research and for allowing me to grow as a research scientist. Your advice on both research as well as on my career have been invaluable. I would also like to thank my mates, Looh George A. and Xiaoyao for being so helpful during this research. Finally, I thank my God, my good Father, for letting me through all the difficulties. I have experienced Your guidance day by day. I will keep on trusting You for my future.